First-principles study on the mechanical and thermodynamic properties of MoNbTaTiW

Uttam Bhandari[1], *Congyan Zhang*[1], *Shengmin Guo*[2], *and Shizhong Yang*[1]

1) Department of Computer Science, Southern University and Agricultural & Mechanical College, Baton Rouge, Louisiana 70813, USA
2) Department of Mechanical and Industrial Engineering, Louisiana State University, Baton Rouge, Louisiana 70803, USA

Abstract: Refractory high-entropy alloys (RHEAs) are emerging as new materials for high temperature structural applications because of their stable mechanical and thermal properties at temperatures higher than 2273 K. In this study, the mechanical properties of MoNbTaTiW RHEA are examined by applying calculations based on first-principles density functional theory (DFT) and using a large unit cell with 100 randomized atoms. The phase calculation of MoNbTaTiW with CALPHAD method shows the existence of a stable body-centered cubic structure at a high temperature and a hexagonal closely packed phase at a low temperature. The predicted phase, shear modulus, Young's modulus, Poisson's ratio, and hardness values are consistent with available experimental results. The linear thermal expansion coefficient, vibrational entropy, and vibrational heat capacity of MoNbTaTiW RHEA are investigated in accordance with Debye–Grüneisen theory. These results may provide a basis for future research related to the application of RHEAs.

Keywords: high-entropy alloy; MoNbTaTiW; mechanical properties; thermodynamic properties; density functional theory

1. Introduction

Since the invention of the first high-entropy alloy (HEA) by Yeh *et al.* [1] in 2004, HEAs have attracted strong interest from both theoretical and experimental scientists. HEAs are metallic alloys made by mixing more than five elements with different contents of each element ranging from 5% to 35%, based on their molar ratios. HEAs are quite different from traditional one-metal element-based alloys. This new alloy design approach can be used to create novel metallic materials with unique properties. For many challenging industrial applications, high strength and good ductility are essential to the mechanical performance of novel HEAs.

Refractory high-entropy alloys (RHEAs) constitute a group of HEAs that incorporate refractory elements, such as Mo, Nb, Ta, Ti, V, W, Re, Zr, and Hf, in constitutional compositions. The fundamental features of RHEAs include an increased temperature strength, reduced density, high melting point, high yield strength, high ductility, and high strain hardening effect [2–5]. Studies on MoNbTaTiW RHEA have been conducted since the discovery of MoNbTaW RHEA. At room temperature, MoNbTaW is very brittle [6]. To increase the strength of MoNbTaW and make it applicable at room

temperature, Han *et al.* [7] added Ti and experimentally studied the properties of MoNbTaTiW RHEA. They reported that the addition of Ti increases the yield strength of MoNbTaW from 996 to 1343 MPa. The measured lattice constant, bulk modulus, shear modulus, and Young's modulus of MoNbTaTiW RHEA are 0.3225 nm, 139 GPa, 59 GPa, and 156 GPa, respectively. Han *et al.* [8] also demonstrated that MoNbTaTiW has a stable body-centered cubic (BCC) phase at a high temperature and exhibits increased strength and ductility at room temperature with Ti addition. Their calculation using the Thermal-Calc software with the TTNI 8 database found that MoNbTaTiW RHEA has a stable BCC structure at high temperatures and a hexagonal closely packed (HCP) phase, which mainly contains Ti, below 640°C.

Mishra *et al.* [9] calculated the elastic and mechanical properties of MoNbTaTiW RHEA by using supercells with 54 and 48 atoms. Cambridge Sequential Total Energy Package is used to optimize geometric supercells. The predicted values of elastic constants, C_{11}, C_{12}, and C_{44}, are 283.44 GPa, 130.50 GPa, and 74.73 GPa, respectively, and the bulk modulus, shear modulus, and Young's modulus of MoNbTaTiW are 193.90 GPa, 70.67 GPa, and 188.00 GPa, respectively. These calculated mechanical properties disagree with the ex-

---

Corresponding author: Shizhong Yang   E-mail: shizhong_yang@subr.edu

🖄 Springer

perimentally measured values mentioned earlier. The disagreement between theoretical and experimental results and the potential of MoNbTaTiW for applications have prompted researchers to further investigate its mechanical and thermal properties. Based on the need for reliable predictive tools for alloy designs, this study demonstrates the capabilities of computational calculations for the prediction of RHEA properties. The mechanical, structural, and phase properties of MoNbTaTiW RHEA are calculated and compared with available experimental results. With the successful demonstration of the computational approach on MoNbTaTiW RHEA, the same methodology can be extended to predict the structural and physical properties of other novel RHEAs.

2. Computational method

The calculation of phase diagrams (CALPHAD) and first-principles calculations are performed in this study. CALPHAD is first performed by employing Thermo-Calc's HEAs database (TCHEA1) [10] provided by Thermo-Calc-2019 software [11]. The calculation based on this database is in good agreement with many experimental reports [12–15]. Thermo-Calc predictions can yield the structure of alloys and do not require any experimental results, such as crystal symmetry and lattice constant. Abu-Odeh *et al.* [16] explained the validation of the TCHEA1 database. The elements in MoNbTaTiW RHEA are equimolar in this study. The first-principles calculations are performed using the Vienna Ab-Initio Simulation Package (VASP 5.4) within the framework of density functional theory (DFT) [17–18] installed in the MedeA software. More information on the MedeA software can be found in a previous publication [19]. The first-principles DFT method has been successfully applied to predict atomic, nano-sized, micrometer-sized, and bulk-sized solid state physical properties. In this study, electron–ion interactions are described by a projector augmented wave (PAW) [20]. The generalized gradient approximation [21] of Perdew–Burke–Ernzerhof [22] is used as an exchange-correlation function to optimize the structure. The convergence criterion is 0.2 eV/nm. The BCC structure of MoNbTaTiW is constructed with the help of a Knuth-shuffle model [23] by using a Python code. The distribution of the constitutional atoms is randomized in the 100-atom supercell model. This model does not have any magnetic moment, and a plane-wave cutoff energy of 500 eV is used. The $4 \times 3 \times 3$ k mesh value comes from the requested k-spacing of 0.02 per nm and corresponds to an actual k-spacing of $0.0173 \times 0.0184 \times 0.0184$ per nm. The 100-atom randomized unit cell model of MoNbTaTiW is shown in Fig. 1.

Elastic constant is calculated on the basis of the stress–strain method of Le Page and Saxe [24–25], which is implemented in the MedeA software. The amount of distortion for each required strain is enough to calculate the elastic

constants. The Voight–Reuss–Hill approximation [26–27] is used in this study to find the mechanical properties of MoNbTaTiW. The mathematical relations for calculating bulk modulus (B), shear modulus (G), Young's modulus (E), and Poisson's ratio (v) are listed in the following equations:
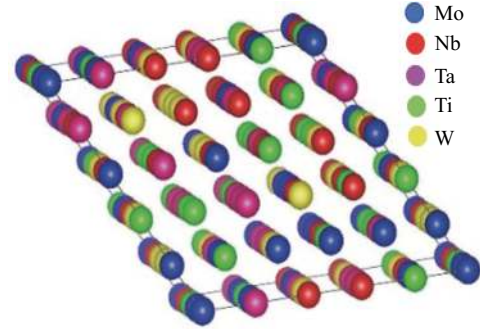

Fig. 1. **Model of a 100-atom randomized unit cell of MoNbTaTiW.**

$$B = \frac{1}{3}(C_{11} + 2C_{12}) \tag{1}$$

$$\begin{cases} G_{\text{Voight}} = \frac{1}{5}(C_{11} - C_{12} + 3C_{44}) \\ G_{\text{Reuss}} = \frac{5}{4(S_{11} - S_{12}) + 3S_{44}} \\ G = \frac{1}{2}(G_{\text{Voight}} + G_{\text{Reuss}}) \end{cases} \tag{2}$$

$$E = \frac{9BG}{3B + G} \tag{3}$$

$$v = \frac{3B - 2G}{2(3B + G)} \tag{4}$$

where C_{11}, C_{12}, and C_{44} are elastic constants, S_{11}, S_{12}, S_{44} are the compliance matrix of G.

Thermodynamic calculations are based on Debye theory. The Grüneisen constant (γ_G) [28] is derived from the pressure–volume equation [29]. The Debye temperature (θ_D) is obtained by using the formula of the mean sound velocity (v_m) as follows:

$$\theta_D = \frac{\hbar}{K_B}\left(\frac{6\pi^2 q}{V_0}\right)^{\frac{1}{3}} v_m \tag{5}$$

where q is the number of atoms in a unit cell, V_0 is the volume, and $\hbar$ and K_B are Planck and Boltzmann constants, respectively.

The lattice contribution to the specific heat capacity (C_V) as a function of temperature (T) is evaluated as:

$$C_v(T) = 9qK_B\left(\frac{T}{\theta_D}\right)^3 \int_0^{x_D} \frac{x^4 \exp x}{(\exp x - 1)^2} dx \tag{6}$$

where $x_D = \frac{\theta_D}{T}$, and θ_D is the Debye temperature. The linear thermal expansion coefficient (α_L) is calculated using the following relation [30]:

$$\alpha_{\text{L}}(T) = \frac{1}{3}\gamma_{\text{G}}\frac{C_{\text{V}}(T)}{BV_0} \tag{7}$$

3. Results and discussion

3.1. Structural and mechanical properties

Phase formation and crystal structures are predicted by calculating the entropy of mixing (ΔS_{mix}), mixing enthalpy (ΔH_{mix}), Ω parameter, atomic packing parameter (γ), and valence electron concentration (VEC) [31–33]. They are defined as follows:

$$\Delta S_{\text{mix}} = -R\sum_{i=1}^{n} C_i \ln C_i \tag{8}$$

$$\Delta H_{\text{mix}} = \sum_{i=1, i\neq j}^{n} 4\Delta H_{ij}^{\text{mix}} C_i C_j \tag{9}$$

$$\begin{cases} \Omega = \dfrac{T_{\text{m}}\Delta S_{\text{mix}}}{|\Delta H_{\text{mix}}|} \\ T_{\text{m}} = C_i(T_{\text{m}})_i \end{cases} \tag{10}$$

$$\begin{cases} \gamma = \dfrac{1 - \sqrt{\dfrac{(r_{\text{s}} + \bar{r})^2 - \bar{r}^2}{(r_{\text{s}} + \bar{r})^2}}}{1 - \sqrt{\dfrac{(r_{\text{L}} + \bar{r})^2 - \bar{r}^2}{(r_{\text{L}} + \bar{r})^2}}} \\ \bar{r} = \sum_{i=1}^{n} C_i r_i \end{cases} \tag{11}$$

$$\text{VEC} = \sum_{i=1}^{n} C_i(\text{VEC})_i \tag{12}$$

where R is the ideal gas constant; n is the number of constituent elements; C_i and C_j are the atomic percentages of the ith and jth elements, respectively; H_{ij}^{mix} is the mixing enthalpy of binary liquid ij alloys; $(T_{\text{m}})_i$ is the melting point of the ith element in K; r_{s} and r_{L} are the smallest and largest atomic sizes of the alloy, respectively; r_i is the atomic radius of the ith element; $(\text{VEC})_i$ is the VEC of the ith element.

The database from Takeuchi and Inoue [34] is used to calculate ΔH_{mix} of MoNbTaTiW RHEA. The calculated ΔH_{mix} of MoNbTaTiW is −5.28 kJ/mol. The calculated structural properties of MoNbTaTiW RHEA are shown in Table 1. According to a previous research [31], the tendency to form a single-phase solid solution of alloy is $\Omega > 1.1$ and $\gamma < 1.175$. The calculated Ω and γ show that MoNbTaTiW satisfies these conditions to form a solid solution. According to previous reports [32–33], alloy forms a stable BCC phase when VEC is less than 6.87. The calculated VEC of MoNbTaTiW RHEA is 5.2. Therefore, MoNbTaTiW RHEA likely forms a stable BCC structure.

Table 1.   Predicted structural properties of MoNbTaTiW at room temperature

ΔS_{mix} / (J·K^{-1}·mol^{-1})	ΔH_{mix} / (kJ·mol^{-1})	T_{m} / K	γ	Ω	VEC
13.38	−5.28	2914	1.079	6.69	5.2

Further information on the phase diagram of MoNbTaTiW RHEA is calculated from the Thermo-Calc software with the TCHEA1 database, which is shown in Fig. 2(a). According to the phase diagram, MoNbTaTiW RHEA has a stable BCC phase over a wide range of temperatures. The melting temperature is found to be 2685 K. When the temperature is below 967 K, the HCP phase precipitates. These findings are in good agreement with those of Han *et al.* [8], who observed that the HCP phase forms below the temperature of 913 K. Han *et al.* [7–8] performed X-ray diffraction experiments and found the stable BCC phase of MoNbTaTiW with a lattice constant of 0.324 nm. Fig. 2(b) represents the Schiel solidification diagram of MoNbTaTiW, which is based on Schiel Gulliver models [35–36]. Equilibrium solidification is represented by a dotted line, whereas solidific-
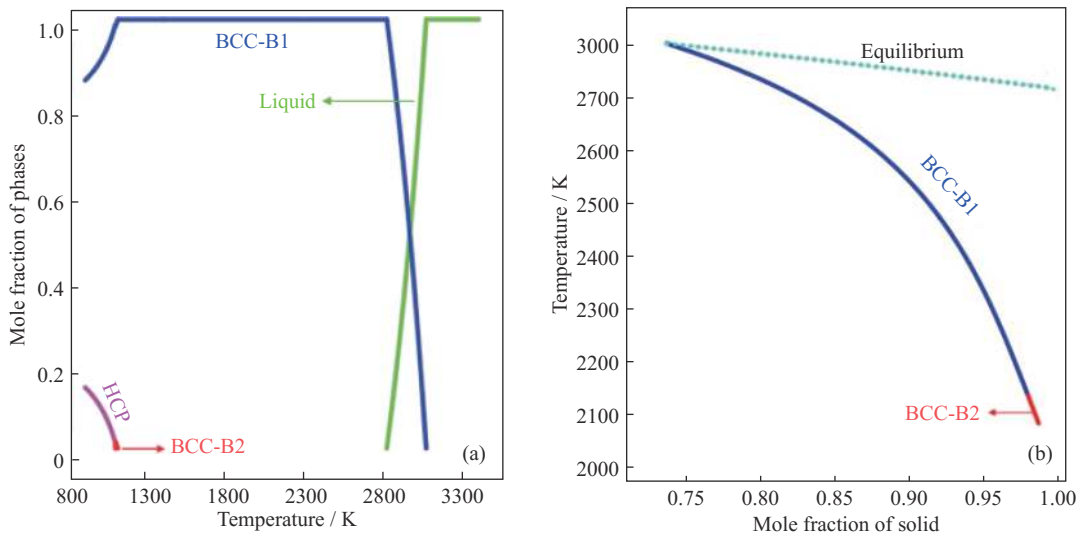

Fig. 2.   Calculated (a) phase diagram and (b) Schiel solidification diagram of MoNbTaTiW.

ation simulation is indicated by a solid line. These two lines diverge at 2753 K, suggesting that segregation occurs in the alloy. This simulation confirms the existence of a stable BCC structure in MoNbTaTiW RHEA until it liquefies at high temperatures. If segregation takes place in alloys, it affects the mechanical and chemical properties of alloys at grain boundaries, which degrade their applications. Experimental results [7–8] also reveal that segregation occurs in alloys because of the presence of ductile elements, such as Ti and Nb, at interdendrite regions, which can hold more strain and increase the comprehensive strain. As a result, segregation minimally affects MoNbTaTiW RHEA. This result demonstrates that Thermo-Calc software can predict the occurrence of segregation with the help of the Schiel solidification dia-

gram. Therefore, Thermo-Calc software is effective in exploring the properties of HEAs and can be very useful in discovering and designing alloys in future studies.

Table 2 shows the single-point equilibrium calculation performed in Thermo-Calc software and presents the compositional components as the mole percentage of elements forming the phases in MoNbTaTiW RHEA at room temperature. The major BCC-B1 phase of MoNbTaTiW mainly comprises Mo, Nb, Ta, and W. Ti has no contribution to the formation of the BCC-B1 phase in MoNbTaTiW. No experimental result regarding the distribution of elements in each phase of MoNbTaTiW can be found in open literature. As such, further experiments are needed to verify the predictions listed in Table 2.

Table 2. Composition components in the mole fraction of elements forming the phases of MoNbTaTiW at room temperature

Phase	Mo	Nb	Ta	Ti	W
BCC-B1	0.25	0.25	0.25	0.00	0.25
HCP	9.66×10^{-9}	3.42×10^{-7}	3.60×10^{-7}	1.00	6.48×10^{-11}

The structural and mechanical properties of MoNbTaTiW obtained through first-principles calculations are listed in Table 3. MoNbTaTiW satisfies the mechanically stable conditions [37] as follows: $C_{44} > 0$; $C_{11} > C_{12}$; $C_{11} + 2C_{12} > 0$. HEA should be ductile and hard for applications. Pugh's criterion [38] is useful to predict the ductility of materials. According to Pugh's criterion, the condition for the ductility of materials is that B/G should be greater than 1.75. MoNbTaW has B/G of 2.51 [39] and 2.04 [9] from first-principles DFT calculations. The B/G of MoNbTaTiW is 3.31, which shows that the ductility of MoNbTaTiW increases because of Ti addition. The experimental result [8] reveals that Ti addition increases the ductility of MoNbTaTiW by 11.5%. The grain

boundary cohesion of MoNbTaTiW increases due to Ti addition, which can overcome intergranular fracture and increase ductility [40–41]. According to previous reports on RHEAs [7,42–43], low VEC can make RHEAs more ductile. The VECs of MoNbTaW and MoNbTaTiW have been calculated to be 5.5 and 5.2, respectively. The VEC of MoNbTaW decreases from 5.5 to 5.2 as Ti added. Moreover, Cauchy pressure ($C_{12} - C_{44}$) is positive in a ductile material and negative in a brittle material [44]. A positive Cauchy pressure of MoNbTaTiW further confirms its ductility nature. The Zener ratio (A_Z) of MoNbTaTiW is 1.06, which reveals its anisotropy nature with a high probability to develop cross-slip pinning [45].

Table 3. Calculated lattice constant (a), three independent elastic stiffness coefficients (C_{11}, C_{12}, and C_{44}), bulk modulus (B), shear modulus (G), Young's modulus (E), Zener ratio (A_Z), Poisson's ratio (v), Pugh's ratio B/G, Vickers hardness (H_V) at zero pressure and kelvin compared with the experimental results [7]

a / nm	C_{11} / GPa	C_{12} / GPa	C_{44} / GPa	B / GPa	G / GPa	E / GPa	A_Z	v	B/G	H_V / GPa	Ref.
0.322	272	163	58	199	60	164	1.06	0.36	3.31	4.34	This work
0.324	—	—	—	139	59	156	—	0.31	—	4.89	[7]

The calculated properties such as lattice constant, shear modulus, Young's modulus, Poisson's ratio, and hardness are in good agreement with the available experimental results [7]. The bulk modulus from the experiment is lower than our predicted value. However, the method of measuring the bulk modulus described by Han *et al.* [7] is unknown. Another 100-atom supercell model based on maximal entropy and initially designed by Lei *et al.* [46] is optimized to test the accuracy of our method for bulk modulus calculation. The third-order Brich–Murnaghan [47] equation of state (EOS) is used through first-principles calculation to obtain the bulk

modulus. Fig. 3 shows the total energy as a function of volume for MoNbTaTiW obtained from the calculation.

The calculated bulk modulus of MoNbTaTiW is found to be 193 GPa via Brich–Murnaghan EOS. The predicted bulk modulus from our supercell is in close agreement with that of the model of Lei *et al.* [46]. Moreover, the bulk modulus calculated by Mishra *et al.* [9] is 193.9 GPa. However, recent experimental studies [7] have shown its value to be 139 GPa, which is almost 60 GPa below our result. Therefore, this bulk modulus should be confirmed through further detailed studies, especially more experiments, in the future.
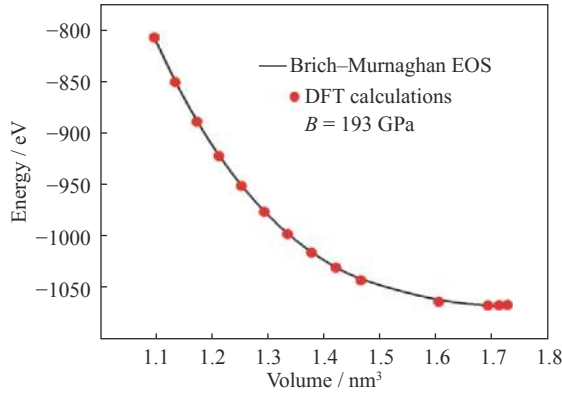
Fig. 3. Total energy as a function of volume in the unit cell of MoNbTaTiW from a maximal entropy model.

3.2. Thermodynamic properties

Debye temperature (θ_D) is an important parameter in describing the covalent bond of solid materials. A material with a high θ_D has a high covalent bond [48]. The calculated θ_D, Grüneisen parameter (γ_G), and v_m of MoNbTaTiW are 295.7 K, 2.23, and 2548 m/s, respectively. Fig. 4(a) shows a calculated curve between temperature and thermal expansion coefficient (α_L). From Fig. 4(a), α_L of MoNbTaTiW increases quickly at a temperature below 300 K and becomes constant as the temperature reaches 600 K. The calculated α_L at 300 and 1500 K of MoNbTaTiW are 8.74×10^{-6} K^{-1} and 9.16×10^{-6} K^{-1}, respectively. Fig. 4(b) presents the relation between temperature and vibrational heat capacity (C_V). C_V increases rapidly at 0–250 K and becomes linear as temperature increases. The linear increment in C_V is mostly caused by lattice vibration. C_V then reaches the Dulong Petit limit at high temperatures. Fig. 4(c) displays temperature against vibrational entropy. Vibrational entropy also increases as temperature rises. All the graphs are calculated at zero pressure. However, no theoretical and experimental reports on the thermodynamic properties of MoNbTaTiW alloys have been presented. Future experimental work is needed to confirm these findings.

4. Conclusion

The first-principles DFT method is utilized to predict the mechanical and thermal properties of MoNbTaTiW RHEA. The phase calculation from Thermo-Calc software shows the existence of a stable BCC phase for MoNbTaTiW. Our elastic calculation reveals that MoNbTaTiW is elastically stable. The calculated Young's modulus, shear modulus, Poisson's ratio, lattice parameter, and hardness are in good agreement with the experimental results. A B/G ratio of 3.31 and a hardness of 4.34 GPa confirm the ductility and hardness of MoNbTaTiW. Our thermodynamic calculations on the thermal expansion coefficient and vibration heat capacity indicate that MoNbTaTiW RHEA is temperature sensitive. In summary,
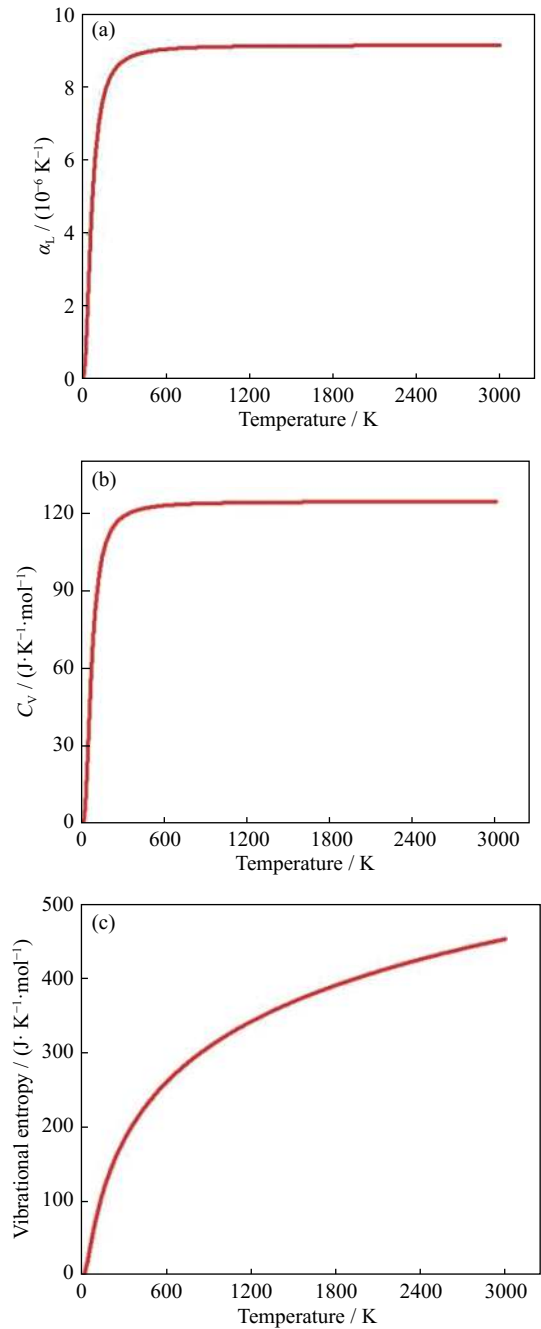

Fig. 4. Temperature against (a) the thermal expansion coefficient (α_L), (b) the vibrational heat capacity (C_V), and (c) the vibrational entropy of MoNbTaTiW.

MoNbTaTiW RHEA may be applied to structural materials in the future because of its outstanding mechanical properties and high thermal stability. The present research may offer a guideline for developing new RHEAs with high hardness and high ductility.

Acknowledgements

References

[1] J.W. Yeh, S.K. Chen, S.J. Lin, J.Y. Gan, T.S. Chin, T.T. Shun, C.H. Tsau, and S.Y. Chang, Nanostructured high-entropy alloys with multiple principal elements: Novel alloy design concepts and outcomes, *Adv. Eng. Mater.*, 6(2004), No. 5, p. 299.

[2] Y.J. Zhou, Y. Zhang, Y.L. Wang, and G.L. Chen, Solid solution alloys of AlCoCrFeNiTi$_x$ with excellent room-temperature mechanical properties, *Appl. Phys. Lett.*, 90(2007), No. 18, art. No. 181904.

[3] M.H. Chuang, M.H. Tsai, W.R. Wang, S.J. Lin, and J.W. Yeh, Microstructure and wear behavior of Al$_x$Co$_{1.5}$CrFeNi$_{1.5}$Ti$_y$ high-entropy alloys, *Acta Mater.*, 59(2011), No. 16, p. 6308.

[4] L.H. Wen, H.C. Kou, J.S. Li, H. Chang, X.Y. Xue, and L. Zhou, Effect of aging temperature on microstructure and properties of AlCoCrCuFeNi high-entropy alloy, *Intermetallics*, 17(2009), No. 4, p. 266.

[5] C.W. Jung, K. Kang, A. Marshal, K.G. Pradeep, J.-B. Seol, H.M. Lee, and P.-P. Choi, Effects of phase composition and elemental partitioning on soft magnetic properties of AlFeCoCrMn high entropy alloys, *Acta Mater.*, 171(2019), p. 31.

[6] O.N. Senkov, G.B. Wilks, J.M. Scott, and D.B. Miracle, Mechanical properties of Nb$_{25}$Mo$_{25}$Ta$_{25}$W$_{25}$ and V$_{20}$Nb$_{20}$Mo$_{20}$Ta$_{20}$W$_{20}$ refractory high entropy alloys, *Intermetallics*, 19(2011), No. 5, p. 698.

[7] Z.D. Han, N. Chen, S.F. Zhao, L.W. Fan, G.N. Yang, Y. Shao, and K.F. Yao, Effect of Ti additions on mechanical properties of NbMoTaW and VNbMoTaW refractory high entropy alloys, *Intermetallics*, 84(2017), p. 153.

[8] Z.D. Han, H.W. Luan, X. Liu, N. Chen, X.Y. Li, Y. Shao, and K.F. Yao, Microstructures and mechanical properties of Ti$_x$NbMoTaW refractory high-entropy alloys, *Mater. Sci. Eng. A*, 712(2018), p. 380.

[9] A. Mishra, G. Priyadarshan, D. Clark, Y. Lu, and R.H. Shi, Theoretical investigations on structural stability and elastic properties of MoNbTaW–*X* (= Ti/V) high entropy alloys, *J. Mater. Sci. Res. Rev.*, 4(2019), No. 2, p. 1.

[10] J.-O. Andersson, T. Helander, L. Höglund, P.F. Shi, and B. Sundman, Thermo-Calc & DICTRA, computational tools for materials science, *Calphad*, 26(2002), No. 2, p. 273.

[11] H. Larsson, A model for 1D multiphase moving phase boundary simulations under local equilibrium conditions, *Calphad*, 47(2014), p. 1.

[12] Y. Lederer, C. Toher, K.S. Vecchio, and S. Curtarolo, The search for high entropy alloys: A high-throughput ab-initio approach, *Acta Mater.*, 159(2018), p. 364.

[13] H.H. Mao, H.L. Chen, and Q. Chen, TCHEA1: A thermodynamic database not limited for "high entropy" alloys, *J. Phase Equilib. Diffus.*, 38(2017), p. 353.

[14] H.L. Chen, H.H. Mao, and Q. Chen, Database development and Calphad calculations for high entropy alloys: Challenges, strategies, and tips, *Mater. Chem. Phys.*, 210(2018), p. 279.

[15] M.C. Gao, B. Zhang, S. Yang, and S.M. Guo, Senary refractory high-entropy alloy HfNbTaTiVZr, *Metall. Mater. Trans. A*, 47(2016), No. 7, p. 3333.

[16] A. Abu-Odeh, E. Galvan, T. Kirk, H. Mao, Q. Chen, P. Mason, R. Malak, and R. Arróyave, Efficient exploration of the high entropy alloy composition-phase space, *Acta Mater.*, 152(2018), p. 41.

[17] P. Hohenberg and W. Kohn, Inhomogeneous electron gas, *Phys. Rev.*, 136(1964), No. 3B, p. B864.

[18] W. Kohn and L.J. Sham, Self-consistent equations including exchange and correlation effects, *Phys. Rev.*, 140(1965), No. 4A, p. A1133.

[19] U. Bhandari, C.Y. Zhang, and S.Z. Yang, Mechanical and thermal properties of low-density Al$_{20+x}$Cr$_{20-x}$Mo$_{20-y}$Ti$_{20}$V$_{20+y}$ alloys, *Crystals*, 10(2020), No. 4, p. 278.

[20] P.E. Blöchl, Projector augmented-wave method, *Phys. Rev. B*, 50(1994), No. 24, p. 17953.

[21] J.P. Perdew, J.A. Chevary, S.H. Vosko, K.A. Jackson, M.R. Pederson, D.J. Singh, and C. Fiolhais, Atoms, molecules, solids, and surfaces: Applications of the generalized gradient approximation for exchange and correlation, *Phys. Rev. B*, 46(1992), No. 11, p. 6671.

[22] J.P. Perdew, K. Burke, and M. Ernzerhof, Generalized gradient approximation made simple, *Phys. Rev. Lett.*, 77(1996), No. 18, p. 3865.

[23] K.E. Donald, *The Art of Computer Programming*, Addison Wesley, Boston, 1968.

[24] Y. Le Page and P. Saxe, Symmetry-general least-squares extraction of elastic coefficients from ab initio total energy calculations, *Phys. Rev. B*, 63(2001), No. 17, art. No. 174103.

[25] Y. Le Page and P. Saxe, Symmetry-general least-squares extraction of elastic data for strained materials from ab initio calculations of stress, *Phys. Rev. B*, 65(2002), No. 10, art. No. 104104.

[26] O.L. Anderson, A simplified method for calculating the debye temperature from elastic constants, *J. Phys. Chem. Solids*, 24(1963), No. 7, p. 909.

[27] K.W. Andrews, Elastic moduli of polycrystalline cubic metals, *J. Phys. D: Appl. Phys.*, 11(1978), No. 18, p. 2527.

[28] F. Drucker, E. Grüneisen, F. Körber, P. Kohnstamm, K. Scheel, E. Schrödinger, F. Simon, J.D. van der Waals, and F. Henning, *Thermische Eigenschaften der Stoffe*, H. Geiger and K. Scheel, eds., Springer, Berlin, 1926.

[29] B. Mayer, H. Anton, E. Bott, M. Methfessel, J. Sticht, J. Harris, and P.C. Schmidt, Ab-initio calculation of the elastic constants and thermal expansion coefficients of Laves phases, *Intermetallics*, 11(2003), No. 1, p. 23.

[30] N.W. Ashcroft and N.D. Mermin, *Solid State Physics*, Saunders College Publishing, Philadelphia, 1976.

[31] X. Yang and Y. Zhang, Prediction of high-entropy stabilized solid-solution in multi-component alloys, *Mater. Chem. Phys.*, 132(2012), No. 2-3, p. 233.

[32] S. Guo, C. Ng, J. Lu, and C.T. Liu, Effect of valence electron concentration on stability of fcc or bcc phase in high entropy alloys, *J. Appl. Phys.*, 109(2011), No. 10, art. No. 103505.

[33] Z.J. Wang, Y.H. Huang, Y. Yang, J.C. Wang, and C.T. Liu, Atomic-size effect and solid solubility of multicomponent alloys, *Scripta Mater.*, 94(2015), p. 28.

[34] A. Takeuchi and A. Inoue, Classification of bulk metallic glasses by atomic size difference, heat of mixing and period of constituent elements and its application to characterization of the main alloying element, *Mater. Trans.*, 46(2005), No. 12, p. 2817.

[35] G.H. Gulliver, The quantitative effect of rapid cooling upon the constitution of binary alloys, *J. Inst. Met*, 9(1913), No. 1, p. 120.

[36] E. Scheil, Bemerkungen zur schichtkristallbildung, *Z. Metallkd.*,

34(1942), No. 3, p. 70.

[37] M. Born and K. Huang, *Dynamical Theory of Crystal Lattices*, Clarendon Press, Oxford, 1956.

[38] S.F. Pugh, XCII. Relations between the elastic moduli and the plastic properties of polycrystalline pure metals, *The London, Edinburgh, and Dublin Philosophical Magazine and Journal of Science*, 45(1954), No. 367, p. 823.

[39] Y.L. Hu, L.H. Bai, Y.G. Tong, D.Y. Deng, X.B. Liang, J. Zhang, Y.J. Li, and Y.X. Chen, First-principle calculation investigation of NbMoTaW based refractory high entropy alloys, *J. Alloys Compd.*, 827(2020), art. No. 153963.

[40] C.T. Liu, J.H. Schneibel, P.J. Maziasz, J.L. Wright, and D.S. Easton, Tensile properties and fracture toughness of TiAl alloys with controlled microstructures, *Intermetallics*, 4(1996), No. 6, p. 429.

[41] J.H. Luan, Z.B. Jiao, W.H. Liu, Z.P. Lu, W.X. Zhao, and C.T. Liu, Compositional and microstructural optimization and mechanical-property enhancement of cast Ti alloys based on Ti–6Al–4V alloy, *Mater. Sci. Eng. A*, 704(2017), p. 91.

[42] Y.D. Wu, Y.H. Cai, X.H. Chen, T. Wang, J.J. Si, L. Wang, Y.D. Wang, and X.D. Hui, Phase composition and solid solution strengthening effect in TiZrNbMoV high-entropy alloys, *Mater. Des.*, 83(2015), p. 651.

[43] C.C. Juan, K.K. Tseng, W.L. Hsu, M.H. Tsai, C.W. Tsai, C.M. Lin, S.K. Chen, S.J. Lin, and J.W. Yeh, Solution strengthening of ductile refractory HfMoxNbTaTiZr high-entropy alloys, *Mater. Lett.*, 175(2016), p. 284.

[44] D. Nguyen-Manh, M. Mrovec, and S.P. Fitzgerald, Dislocation driven problems in atomistic modelling of materials, *Mater. Trans.*, 49(2008), No. 11, p. 2497.

[45] V. Tvergaard and J.W. Hutchinson, Microcracking in ceramics induced by thermal expansion or elastic anisotropy, *J. Am. Ceram. Soc.*, 71(1988), No. 3, p. 157.

[46] J. Lei, S. Guo, E. Khosravi, and S. Yang, The stability and stiffness of TaNbHfZrTi alloy from first principles simulation, [in] *Materials Science & Technology 2012 (MS&T'12) Conference Proceedings*, Pittsburgh, 2012, p. 196.

[47] F. Birch, Finite elastic strain of cubic crystals, *Phys. Rev.*, 71(1947), No. 11, p. 809.

[48] S. Wang, Y.H. Zhao, H. Hou, Z.Q. Wen, P.L. Zhang, and J.Q. Liang, Effect of anti-site point defects on the mechanical and thermodynamic properties of $MgZn_2$, $MgCu_2$ Laves phases: A first-principle study, *J. Solid State Chem.*, 263(2018), p. 18.